

Local field inhomogeneity and ferroelectric switching dynamics in $\text{Hf}_{1-x}\text{Zr}_x\text{O}_2$ thin films

M. S. Song , K. C. Lee, J. C. Choi, K. Lee , and S. C. Chae *

Department of Physics Education, Seoul National University, Seoul 08826, Korea



(Received 7 September 2021; accepted 10 November 2021; published 23 November 2021)

We report on the inhomogeneity of the internal bias according to the Zr alloy concentration confirmed by the ferroelectric switching dynamics of $\text{Hf}_{1-x}\text{Zr}_x\text{O}_2$ thin films. The analytic model for the internal bias was considered in terms of the dipole-dipole interaction accompanied by Zr concentration variation. The ferroelectricity and switching dynamics of $\text{Hf}_{1-x}\text{Zr}_x\text{O}_2$ thin films were investigated using conventional electrical measurements and local piezoresponse microscopy. Analysis of static and dynamic polarization reversal revealed a correlation between the activation field for polarization switching and Zr concentrations through the variation in local ferroelectric coercivity and the characteristic ferroelectric switching time. The spatially inhomogeneous local built-in electric field was attributed to the defect interaction in the $\text{Hf}_{1-x}\text{Zr}_x\text{O}_2$ thin films.

DOI: [10.1103/PhysRevMaterials.5.114408](https://doi.org/10.1103/PhysRevMaterials.5.114408)

I. INTRODUCTION

Fluorite-structured HfO_2 thin films are of interest for dramatic observation and the rich aspect of ferroelectricity for device applications [1–5]. The ferroelectricity in HfO_2 thin films originates from the noncentrosymmetric orthorhombic phase, namely, the $Pca2_1$ phase, which was first reported in 2011 [1]. In the case of fluorite structures, depending on surface energy, the orthorhombic (ferroelectric) phase can be stabilized even in the ultrathin region [6,7]. Robust ferroelectricity in sub-10 nm thick films and strong complementary metal-oxide semiconductor (CMOS) compatibility with high scalability have attracted vast scientific and industrial interest [3]. Most research efforts have been devoted to the fast operation of transistor devices beyond the thermodynamic limit with negative capacitance and the development of nonvolatile memory devices such as ferroelectric field effect transistors (FeFETs) [8–11]. The steep increase in operation current exceeding the thermodynamic limit of 60 mV per decade has been attributed to the negative capacitance in the heterostructure of HfO_2 with other dielectrics [8]. Ferroelectricity based on flat ferroelectric phonons also demonstrated the scale-free nature of ferroelectric HfO_2 for the ultimate density of nonvolatile ferroelectric memory [11]. Both the negative capacitance and the distinct origin of the ferroelectricity of HfO_2 thin films require a concrete understanding of dynamic characteristic features during the reversal of ferroelectric polarization.

Ferroelectric switching dynamics was analyzed to identify the unique characteristics of ferroelectricity [12–14]. Ferroelectric polarization reversal of high-quality epitaxial ferroelectrics was successfully explained by the Kolmogorov-Avrami-Ishibashi (KAI) model, where the conventional extrinsic switching model was described as the formation of a nucleus followed by movement of the domain walls [15].

During ferroelectric polarization reversal, however, inevitable broadening of the characteristic time, i.e., the ferroelectric switching time of the polarization flip along the external bias, represents the inhomogeneity contributing to polarization switching [16]. Various attempts, including nucleation-limited switching and/or inhomogeneous fields based on the empirical Gaussian distribution of a local electric field, have unveiled the distinct feature of ferroelectricity in a fluorite ferroelectric, e.g., the intrinsic character of the wake-up phenomena [12,13]. Lee *et al.* elucidated the role of artifact density in films during external field cycling corresponding to the wake-up behavior with retardation of the ferroelectric characteristic switching time [13]. Hyun *et al.* argued the hard ferroelectricity of $\text{Hf}_{0.5}\text{Zr}_{0.5}\text{O}_2$ compared to conventional perovskite ferroelectric materials in terms of the activation field and characteristic switching time [12]. However, the uncertainty of the origin of the expansion of the characteristic switching time distribution can mislead causal interpretations of experimental observations. Here, we deduced that the local field distribution stemmed from the dipole-dipole interaction in the disordered system and we report the switching dynamics of a ferroelectric $\text{Hf}_{1-x}\text{Zr}_x\text{O}_2$ film series through this analytical model based on the defect dipole interaction superimposed on ferroelectric switching. We found that the Zr concentration contributes to the inhomogeneity of the local field, which deforms the polarization switching behavior at both macroscopic and microscopic scales.

II. SAMPLES AND EXPERIMENT

We prepared $\text{Hf}_{1-x}\text{Zr}_x\text{O}_2$ thin films to investigate ferroelectric properties according to differences in Zr concentrations. To fabricate the ferroelectric $\text{Hf}_{1-x}\text{Zr}_x\text{O}_2$ capacitor structure, a 10 nm thick bottom TiN electrode was deposited on a silicon substrate by DC sputtering. Ferroelectric $\text{Hf}_{1-x}\text{Zr}_x\text{O}_2$ films were fabricated using atomic layer deposition at 280 °C with tetrakis(ethylmethylamido) hafnium (TEMAH), tetrakis(ethylmethylamido) zirconium (TEMAZ),

*scchae@snu.ac.kr

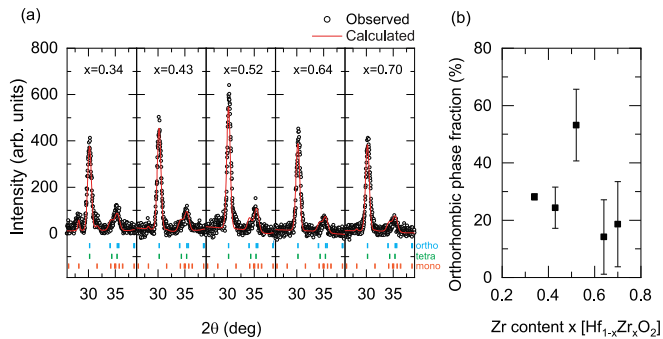


FIG. 1. Structural analysis of $\text{Hf}_{1-x}\text{Zr}_x\text{O}_2$ thin films using x-ray diffraction. (a) Rietveld refinement of the grazing incident x-ray diffraction plot of $\text{Hf}_{1-x}\text{Zr}_x\text{O}_2$ thin films with x values from 0.34 to 0.70 with measured data (black dots) and simulated curves (red line). (b) The orthorhombic phase fraction of the $\text{Hf}_{1-x}\text{Zr}_x\text{O}_2$ thin films estimated by Rietveld analysis.

and ozone as the Hf precursor, Zr precursor, and oxygen source, respectively. By varying the cycle ratio of atomic layer deposition, polycrystalline $\text{Hf}_{1-x}\text{Zr}_x\text{O}_2$ films were prepared with x values of 0.34, 0.43, 0.52, 0.64, and 0.70, which were confirmed by x-ray photoemission spectroscopy. To measure the electric properties, TiN top electrodes with a size of $90\ \mu\text{m} \times 90\ \mu\text{m}$ were deposited on the $\text{Hf}_{1-x}\text{Zr}_x\text{O}_2$ film by DC sputtering. The prepared specimens were postannealed at 650°C for 20 s in ambient N_2 for crystallization into ferroelectric $\text{Hf}_{1-x}\text{Zr}_x\text{O}_2$ films. Polarization-voltage hysteresis and time-dependent dynamic polarization switching $P(t)$ were measured using a conventional semiconductor parameter analyzer (Keithley 4200) and a ferroelectric tester (TF Analyzer 3000, aixACCT Systems). Capacitance-voltage measurements were performed using an impedance analyzer (Model E4990A, Keysight).

III. RESULTS AND DISCUSSION

A. Film characterization

$\text{Hf}_{1-x}\text{Zr}_x\text{O}_2$ thin films with varying Zr concentrations exhibited systematic structural phase variation comprising orthorhombic/tetragonal and monoclinic phases. Figure 1(a) shows the grazing incident x-ray diffraction patterns of $\text{Hf}_{1-x}\text{Zr}_x\text{O}_2$ films with $x = 0.34, 0.43, 0.52, 0.64,$ and 0.70 . Rietveld refinements denoted by the red solid lines in Fig. 1(a) were carried out to analyze the crystal structure of polycrystalline $\text{Hf}_{1-x}\text{Zr}_x\text{O}_2$ thin films. All the specimens exhibited the polycrystallinity of ferroelectric orthorhombic and non-ferroelectric monoclinic/tetragonal phase mixtures. With an increasing Zr content, clear shrinkage of the monoclinic phase was observed with annihilation of peak intensities near $\sim 28.2^\circ$ and $\sim 31.6^\circ$ corresponding to the monoclinic (11) and monoclinic (111) peaks, respectively. On the other hand, the orthorhombic structural phase is enhanced primarily by a Zr concentration of 0.52, as depicted in Fig. 1(b). The previous reports about the analysis of crystallinity of ferroelectric HfO_2 film demonstrated that the orthorhombic phase dominates at the Hf and Zr concentration of ~ 0.5 [17]. However, note that the estimated fraction of the orthorhombic phase only can

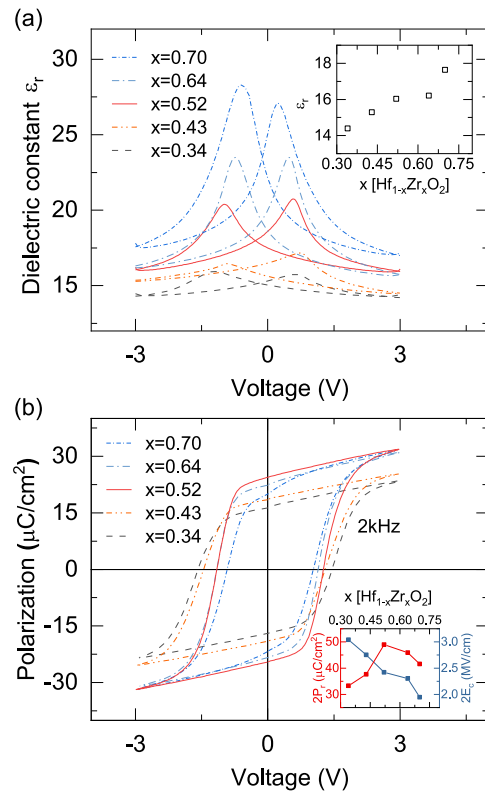


FIG. 2. (a) Hysteresis of the relative permittivity ϵ_r of $\text{Hf}_{1-x}\text{Zr}_x\text{O}_2$ thin films with x values from 0.34 to 0.70. The inset shows the dielectric constant of the nonswitched part at the end of the curve (empty black squares). (b) Polarization-voltage hysteresis of $\text{Hf}_{1-x}\text{Zr}_x\text{O}_2$ thin films with x values from 0.34 to 0.70. The inset shows the extracted coercive field (solid blue squares) and polarization (solid red squares) values.

indicate the tendency for the change of structure phase in HZO thin films, regarding the limited analysis range and extrinsic effect in the thin film structure [18,19].

The ferroelectricity of the $\text{Hf}_{1-x}\text{Zr}_x\text{O}_2$ thin films exhibited systematic modulation of the dielectric and ferroelectric properties. Figures 2(a) and 2(b) show the capacitance-voltage (C - V) curves and polarization-voltage (P - V) hysteresis curves for 10 nm thick $\text{Hf}_{1-x}\text{Zr}_x\text{O}_2$ films with varying zirconium concentrations, respectively. The C - V characteristics were measured with a small AC voltage signal of 1 MHz and 50 mV amplitude after each of 10^5 training cycles by 3.0 V, 2 kHz triangle pulses. As the Zr concentration increased, the dielectric constant outside the peak region exhibited a steady incline from approximately 14 to 18, as shown in the inset of Fig. 2(a). The dielectric constant outside the peak represents the static dielectric contribution, while the peaks in the butterflylike hysteresis in relative permittivity result from ferroelectric polarization switching [20]. The dielectric constants of the monoclinic, orthorhombic, and tetragonal phases are known to theoretically be 19–25, 24–29, and 24–57, respectively [21,22]. The increase in the dielectric constant implies that the nonferroelectric monoclinic phase was relatively decreased and the orthorhombic/tetragonal phases were enhanced with increasing Zr concentrations. Meanwhile, a systematic change in the P - V curve was also observed along

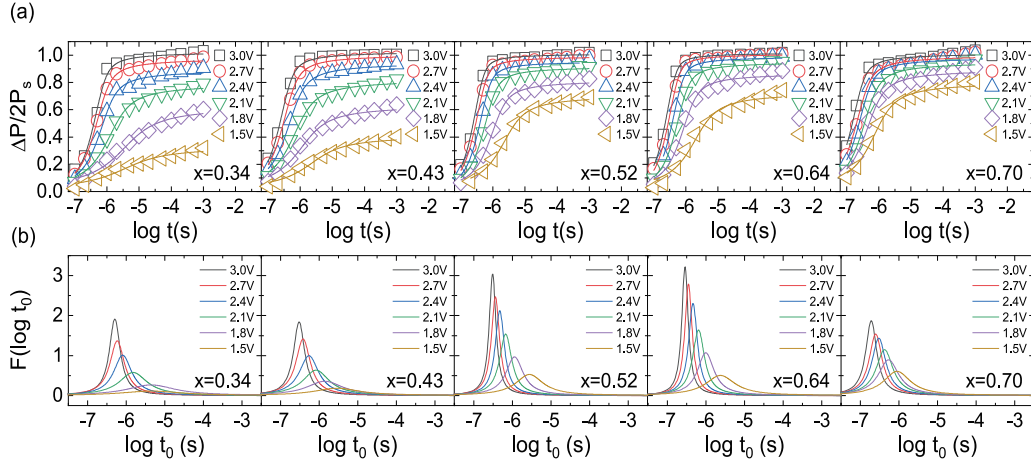


FIG. 3. Ferroelectric switching dynamics of $\text{Hf}_{1-x}\text{Zr}_x\text{O}_2$ thin films. (a) Time dependence of the polarization flip $\Delta P(t)$ of $\text{Hf}_{1-x}\text{Zr}_x\text{O}_2$ thin films under various external voltages V_{ext} . (b) The distribution functions $F(\log t_0)$ of the logarithmic characteristic switching time t_0 .

with a change in the Zr concentration, as shown in Fig. 2(b). After 10^5 training cycles by 3.0 V, 2 kHz triangle pulses corresponding to the wake-up process [23], the remnant polarization value $2P_r$ with different x values of 0.34, 0.43, 0.52, 0.64, and 0.70 were measured to be 33.2, 37.3, 48.9, 45.6, and 41.9 $\mu\text{C}/\text{cm}^2$, respectively, as shown in the inset of Fig. 2(b). Notably, the $\text{Hf}_{0.48}\text{Zr}_{0.52}\text{O}_2$ film showed the highest P_r value, which is consistent with the orthorhombic phase fraction estimated from x-ray diffraction and previously reported works [24]. In addition, the P - V hysteresis loops changed from a nearly square shape to an oblique shape as the Zr concentration became farther from the $x = 0.52$ sample, which may have been caused by a change in the ferroelectric domain switching dynamics [25].

B. Ferroelectric switching dynamics model

In practical dielectric materials, the inevitable defects can affect the switching of the spontaneous ferroelectric polarization. The presence of defect dipoles in ferroelectric materials imposes the conventional dipole-dipole interaction of $E_d = V_p \frac{3\tilde{r}(m)-m}{r^3} \equiv V_p \frac{\tilde{E}_d}{r^3}$, where V_p , r , and m are the particle volume, location of a particle, and dipole moment, respectively. For a dilute system where all spatial correlations can be neglected, the internal field distribution created by N particles in system volume V can be expressed as the superposition of individual dipole-dipole interaction fields [26,27]:

$$F(E_d) = \frac{1}{V^N} \int \delta \left[E_d - \sum_{i=1}^N E_d(m_i, r_i) \right] \prod_{i=1}^N d^3 r_i. \quad (1)$$

Using the Fourier transform, we can obtain the form

$$F(k) \simeq \exp \left(-\frac{|k|NV_p}{V} \right) \sim \exp(-\Gamma|k|). \quad (2)$$

This exponential decay represents a Lorentzian distribution of dipole interaction fields, $F(E_d) = C \left(\frac{\Gamma^2}{E_d^2 + \Gamma^2} \right)$, with the inverse Fourier transform of $\exp(-\Gamma|k|)$. Here, C is the normalization constant, and Γ represents the inhomogeneity of the local field which depends on the particle volume fraction. Investigation of the distribution function of the local field derived from a randomly distributed field based on the

dipole-dipole interaction revealed the interaction local field distribution in a disordered system and the effect of dipole defects on the deformed hysteresis in both electric and magnetic systems [13,14,27–29].

The Lorentzian distribution of local fields can be associated with the Lorentzian distribution of the characteristic ferroelectric switching time. In the low external field E_{ext} region, polarization switching should be governed by a thermal activation process at the pinning sites. Without the effect of the local field, thermal activation results in a domain-wall speed in the form of $v \propto 1/t_0 \propto \exp[-(\frac{U}{k_B T})(\frac{E_0}{E_{ext}})]$, where U is the energy barrier and E_0 is the threshold electric field for pinned domains [30]. With the local field effect on domain-wall motion in light of the thermal activation process, the associated t_0 can be expressed as $t_0 \sim \exp[(\frac{U}{k_B T})(\frac{E_0}{E_{ext} + E_d})]$ such that the distribution of the local field E_d results in a distribution in $\log t_0$ using the relation $F(\log t_0) = F(E_d) |dE_d(\log t_0)/d(\log t_0)|$ with $\log t_0 \approx \frac{UE_0}{k_B T} (\frac{1}{E_{ext}}) \equiv \alpha (\frac{1}{E_{ext}})$, and the distribution for switching time is $w \approx \frac{UE_0 \Gamma}{k_B T} (\frac{1}{E_{ext}^2}) = \alpha \Gamma (\frac{1}{E_{ext}^2})$ [31]. Therefore, the Lorentzian distribution for switching time can express the field distribution originating from defect dipoles in terms of the activation field α and the inhomogeneity of the local field Γ .

To explore changes in the remnant polarization and the inhomogeneity of the switching field, ferroelectric switching dynamics were analyzed in terms of variation in the characteristic switching time. Figure 3(a) shows the $\Delta P(t)/2P_s$ values as a function of logarithmic time for each of the woken-up $\text{Hf}_{1-x}\text{Zr}_x\text{O}_2$ thin films with different external voltages V_{ext} at room temperature. All the specimens exhibited coherent polarization switching along the external field. The measured $\Delta P(t)/2P_s$ values were analyzed with ferroelectric seed nucleation and domain-wall motion with variation in the characteristic switching time with a Lorentzian distribution as follows [31],

$$\frac{\Delta P(t)}{2P_s} = \int \left[1 - \exp \left\{ -\left(\frac{t}{t_0} \right)^2 \right\} \right] F(\log t_0) d(\log t_0), \quad (3)$$

$$F(\log t_0) = \frac{A}{\pi} \left[\frac{w}{(\log t_0 - \log t_1)^2 + w^2} \right], \quad (4)$$

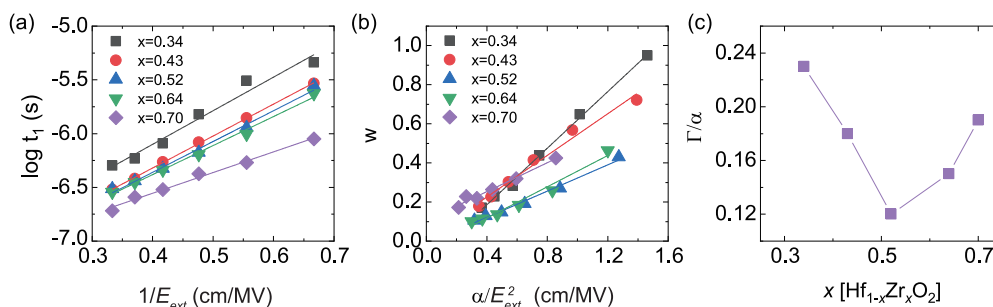


FIG. 4. The external electric field (E_{ext})–dependent (a) characteristic switching time and (b) full width at half maximum value of the distribution with various Zr contents. (c) The ratio of activation field α and half width Γ at half maximum of local field distributions with a Zr concentration change.

where A , w , and $\log t_1$ are a normalization constant, the half width at half maximum of the distribution, and the mean distribution value, respectively. Note that a nucleation-limited switching model has been proposed to account for polarization switching as an ensemble of elementary regions that switch independently with a distribution of switching time [16]. The variation in each region with different switching times can be considered a by-product of the variation in the internal local field in the film. Figure 3(b) shows the extracted Lorentzian distribution used for the model fit of switching dynamics in Fig. 3(a). The peak sharpness represented by the full width at half maximum (FWHM) value was enhanced mostly in the Hf_{0.48}Zr_{0.52}O₂ film.

The Hf_{1-x}Zr_xO₂ thin film with a symmetric composition ratio had the lowest inhomogeneity of built-in electric fields caused by various defects compared to films with other composition ratios. Figures 4(a) and 4(b) show the characteristic switching time $\log(t)$ as a function of $1/E_{ext}$ and a plot of w versus α/E_{ext}^2 for Hf_{1-x}Zr_xO₂ films with various x values, respectively. The linearity in the characteristic switching time

$\log(t)$ as a function of $1/E_{ext}$ clearly indicates that ferroelectric switching under an external applied voltage is governed by the thermal activation process. The activation field α for ferroelectric switching decreased from 3.13 to 1.93 eV/cm as the Zr concentration increased. On the other hand, the peak broadness Γ of the Lorentzian distribution obtained from the linear fit of the FWHM of the Lorentzian distribution as a function of $1/E_{ext}^2$ shows a minimum value with the $x = 0.52$ sample, as shown in Fig. 4(b), implying that the fluctuation of the required switching field due to the defect dipole interaction in the entire specimen, i.e., Γ/α , is lowest with the $x = 0.52$ sample, as shown in Fig. 4(c).

C. Local field inhomogeneity

The Hf_{1-x}Zr_xO₂ thin film with a symmetric composition ratio exhibited steep local piezoresponse hysteresis for abrupt piezoelectric switching behavior. Figures 5(a)–5(c) show piezoresponse spectroscopy results for the Hf_{1-x}Zr_xO₂ thin films with various x values of 0.34, 0.52, and 0.70,

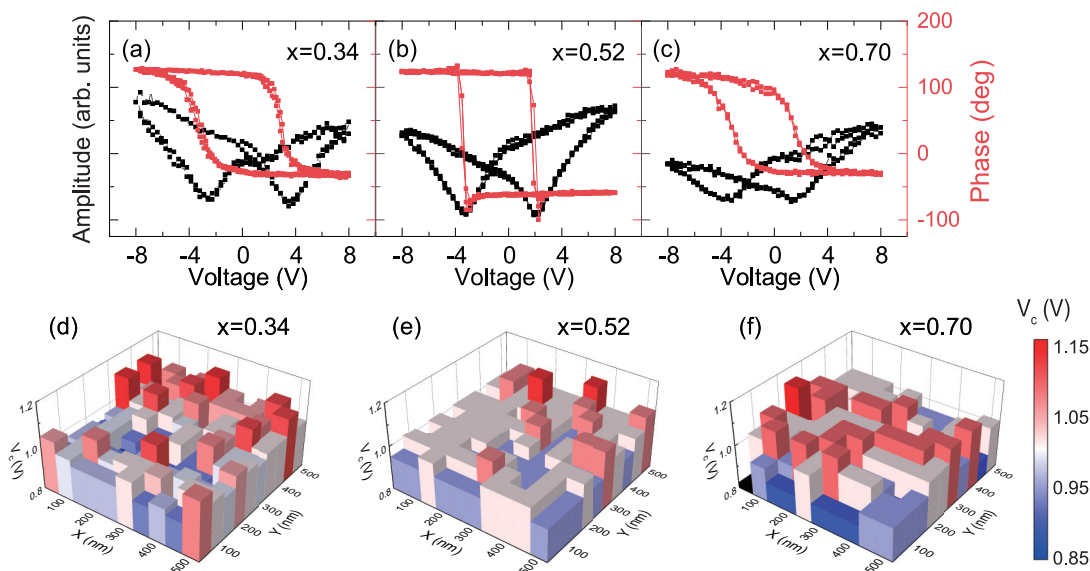


FIG. 5. Local piezoresponse and coercive voltage distribution of the Hf_{1-x}Zr_xO₂ thin films. The piezoresponse hysteresis amplitude (solid black squares) and phase (solid red squares) for (a) Hf_{0.66}Zr_{0.34}O₂, (b) Hf_{0.48}Zr_{0.52}O₂, and (c) Hf_{0.30}Zr_{0.70}O₂. The hysteresis loops were collected in arrays of 10×10 points covering an area of $0.5 \times 0.5 \mu\text{m}^2$, with regular spacing of 50 nm between the adjacent nodes of the grid. Coercive voltage distributions of (d) Hf_{0.66}Zr_{0.34}O₂, (e) Hf_{0.48}Zr_{0.52}O₂, and (f) Hf_{0.30}Zr_{0.70}O₂, respectively.

respectively. Clear hysteresis was observed in the amplitude and phase of the piezoresponse, with a local coercivity of ~ 3 to ~ 2.5 V and transient 180° phase shifts corresponding to piezoelectric switching. For the higher coercivity in the piezoresponse hysteresis, the reduced effective field due to the improper contact between bare surface and conductive tip can be considered. Note that the abruptness of the piezoelectric hysteresis associated with the local switching homogeneity showed the most sudden piezoresponse flip in the $x = 0.52$ sample.

To verify local field fluctuation with different Zr concentrations, hysteresis loops were tested and collected in arrays of 10×10 points covering an area of $0.5 \times 0.5 \mu\text{m}^2$, with a regular spacing of 50 nm between the adjacent nodes of the grid. The piezoresponse coercive voltage maps for each individual point of the grid provide a direct view into the spatial variation in switching inhomogeneities across the surface. The coercivity maps extracted from the arrays of piezoelectric hysteresis loops with different Zr concentrations are shown in Figs. 5(d)–5(f). The color variation in Figs. 5(d)–5(f) indicates spatial inhomogeneity of coercivity for piezoelectric switching. Notably, the $\text{Hf}_{0.48}\text{Zr}_{0.52}\text{O}_2$ film had lower switching inhomogeneity than the other films, indicating that the local field fluctuation decreased with the $x = 0.52$ sample.

Considering the ferroelectric switching dynamics and direct imaging of the spatial distribution of the piezoelectric response coercive voltage, the symmetrically stoichiometric alloy of the $\text{Hf}_{1-x}\text{Zr}_x\text{O}_2$ thin film showed the lowest fluctuation of the local electric field. The key element for ferroelectric polarization switching with low external stimulation is the thermal activation process with finite activation field/energy, which is strongly related to ferroelectric nucleation and/or domain-wall motion by pinning-depinning processes at defect sites [32]. In the case of doped ferroelectric HfO_2 thin films, various defects including competing non-ferroelectric phase, oxygen vacancies, charged defects, and domain orientations can be existing in the film and contribute to the ferroelectric properties [12,13,23,33,34]. Analysis of ferroelectric switching dynamics in terms of local field fluctuations indicated that the defect dipole interaction during the entire ferroelectric switching process of $\text{Hf}_{1-x}\text{Zr}_x\text{O}_2$ film crystallized at high temperature was restricted as the Zr concentration approached approximately 0.52. Restriction of local field fluctuation was also identified in the spatial investigation of local coercivity using piezo force microscopy, where each individual point of the grid provides a direct view into the spatial variation in the switching coercivities. Through the spatial variation in the local coercive voltage and the ferroelectric switching dynamics, the fluctuation of the required switching field Γ/α associated with the variation in ferroelectric hysteresis depending on Zr concentration can be attributed to the microscopic inhomogeneity of the local field due to the defect dipole interaction, as schematically shown in Fig. 6. The previous studies comprehended the

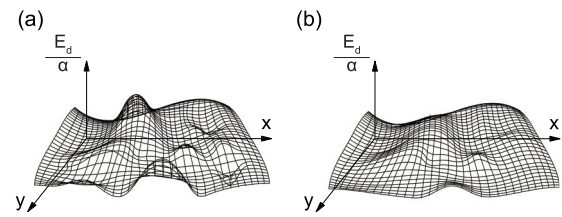


FIG. 6. Schematic diagrams of normalized local field distributions with (a) inhomogeneous local fields and (b) uniform local fields.

ferroelectric switching behavior related to the local field distribution and activation field separately [12,13,35,36]. However, considering the contribution of local field distribution to the ferroelectric switching, the relative ratio between local field variation and the activation field will govern the ferroelectric polarization switching. Even the small local field could impede the ferroelectric switching depending on the relative ratio to the activation field. Thus, the enhanced homogeneity of local field fluctuation Γ/α depending on the Zr concentration can be interpreted as the key element for reliable ferroelectric switching in fluorite structure-based ferroelectricity.

IV. CONCLUSION

In summary, we investigated the local field fluctuation and subsequent ferroelectric switching dynamics of polycrystalline $\text{Hf}_{1-x}\text{Zr}_x\text{O}_2$ thin films with various Zr concentrations. The ferroelectric switching characteristics of the polycrystalline $\text{Hf}_{1-x}\text{Zr}_x\text{O}_2$ thin films with various Zr concentrations exhibited variations in ferroelectric coercivity and ferroelectric characteristic switching time. These changes were analyzed in terms of the variation in built-in local fields associated with the defect dipole interactions. In addition, the spatial microscopic investigation of local piezoresponse coercivity fluctuation showed that the $\text{Hf}_{0.48}\text{Zr}_{0.52}\text{O}_2$ film had the lowest local field inhomogeneity, which is consistent with the argument of internal bias revealed in the variation in ferroelectric switching dynamics.

ACKNOWLEDGMENTS

This study was supported by the Ministry of Trade, Industry, and Energy of Korea (Grant No. 10080657), the Korea Semiconductor Research Consortium program for the development of future semiconductor devices, and the National Research Foundation of Korea (NRF) grant funded by the Korea government (MSIT) (Grants No. NRF-2020M3F3A2A01081594, No. 2021R1A2C1094795). Part of this study was performed using the facilities of the IBS Center for Correlated Electron Systems, Seoul National University.

[1] T. Böske, J. Müller, D. Bräuhäus, U. Schröder, and U. Böttger, *Appl. Phys. Lett.* **99**, 102903 (2011).

[2] B. Zeng, C. Liu, S. Dai, P. Zhou, K. Bao, S. Zheng, Q. Peng, J. Xiang, J. Gao, J. Zhao *et al.*, *Adv. Funct. Mater.* **31**, 2011077 (2021).

- [3] U. Schroeder, S. Mueller, J. Mueller, E. Yurchuk, D. Martin, C. Adelman, T. Schloesser, R. van Bentum, and T. Mikolajick, *ECS J. Solid State Sci. Technol.* **2**, N69 (2013).
- [4] B. Zeng, M. Liao, Q. Peng, W. Xiao, J. Liao, S. Zheng, and Y. Zhou, *IEEE J. Electron Devices Soc.* **7**, 551 (2019).
- [5] S. J. Kim, J. Mohan, J. S. Lee, H. S. Kim, J. Lee, C. D. Young, L. Colombo, S. R. Summerfelt, T. San, and J. Kim, *ACS Appl. Mater. Interfaces* **11**, 5208 (2019).
- [6] S. S. Cheema, D. Kwon, N. Shanker, R. dos Reis, S.-L. Hsu, J. Xiao, H. Zhang, R. Wagner, A. Datar, M. R. McCarter *et al.*, *Nature (London)* **580**, 478 (2020).
- [7] M. Hoffmann, U. Schroeder, T. Schenk, T. Shimizu, H. Funakubo, O. Sakata, D. Pohl, M. Drescher, C. Adelman, R. Materlik *et al.*, *J. Appl. Phys.* **118**, 072006 (2015).
- [8] S. Salahuddin and S. Datta, *Nano Lett.* **8**, 405 (2008).
- [9] M. Hoffmann, M. Pešić, K. Chatterjee, A. I. Khan, S. Salahuddin, S. Slesazeck, U. Schroeder, and T. Mikolajick, *Adv. Funct. Mater.* **26**, 8643 (2016).
- [10] A. I. Khan, K. Chatterjee, B. Wang, S. Drapcho, L. You, C. Serrao, S. R. Bakaul, R. Ramesh, and S. Salahuddin, *Nat. Mater.* **14**, 182 (2015).
- [11] H.-J. Lee, M. Lee, K. Lee, J. Jo, H. Yang, Y. Kim, S. C. Chae, U. Waghmare, and J. H. Lee, *Science* **369**, 1343 (2020).
- [12] S. D. Hyun, H. W. Park, Y. J. Kim, M. H. Park, Y. H. Lee, H. J. Kim, Y. J. Kwon, T. Moon, K. D. Kim, and Y. B. Lee, *ACS Appl. Mater. Interfaces* **10**, 35374 (2018).
- [13] T. Y. Lee, K. Lee, H. H. Lim, M. S. Song, S. M. Yang, H. K. Yoo, D. I. Suh, Z. Zhu, A. Yoon, M. R. MacDonald *et al.*, *ACS Appl. Mater. Interfaces* **11**, 3142 (2019).
- [14] M. S. Song, T. Y. Lee, K. Lee, K. C. Lee, and S. C. Chae, *Appl. Phys. Lett.* **117**, 162903 (2020).
- [15] Y. Ishibashi and Y. Takagi, *J. Phys. Soc. Jpn.* **31**, 506 (1971).
- [16] A. K. Tagantsev, I. Stolichnov, N. Setter, J. S. Cross, and M. Tsukada, *Phys. Rev. B* **66**, 214109 (2002).
- [17] M. H. Park, Y. H. Lee, H. J. Kim, T. Schenk, W. Lee, K. Do Kim, F. P. Fengler, T. Mikolajick, U. Schroeder, and C. S. Hwang, *Nanoscale* **9**, 9973 (2017).
- [18] M. H. Park, T. Schenk, C. M. Fancher, E. D. Grimley, C. Zhou, C. Richter, J. M. LeBeau, J. L. Jones, T. Mikolajick, and U. Schroeder, *J. Mater. Chem. C* **5**, 4677 (2017).
- [19] L. B. McCusker, R. B. Von Dreele, D. E. Cox, D. Louer, and P. Scardi, *J. Appl. Crystallogr.* **32**, 36 (1999).
- [20] L. Pintilie, M. Lisca, and M. Alexe, *Appl. Phys. Lett.* **86**, 192902 (2005).
- [21] R. Materlik, C. Künneth, and A. Kersch, *J. Appl. Phys.* **117**, 134109 (2015).
- [22] C. Adelman, H. Tielens, D. Dewulf, A. Hardy, D. Pierreux, J. Swerts, E. Rosseel, X. Shi, M. Van Bael, and J. Kittl, *J. Electrochem. Soc.* **157**, G105 (2010).
- [23] D. Zhou, J. Xu, Q. Li, Y. Guan, F. Cao, X. Dong, J. Müller, T. Schenk, and U. Schröder, *Appl. Phys. Lett.* **103**, 192904 (2013).
- [24] J. Muller, T. S. Boscke, U. Schroeder, S. Mueller, D. Brauhaus, U. Bottger, L. Frey, and T. Mikolajick, *Nano Lett.* **12**, 4318 (2012).
- [25] J. Y. Jo, S. M. Yang, H. S. Han, D. J. Kim, W. S. Choi, T. W. Noh, T. K. Song, J.-G. Yoon, C.-Y. Koo, J.-H. Cheon *et al.*, *Appl. Phys. Lett.* **92**, 012917 (2008).
- [26] M. W. Klein, *Phys. Rev.* **173**, 552 (1968).
- [27] D. V. Berkov, *Phys. Rev. B* **53**, 731 (1996).
- [28] R. Walstedt and L. Walker, *Phys. Rev. B* **9**, 4857 (1974).
- [29] D. A. Drabold and P. A. Fedders, *Phys. Rev. B* **37**, 3440 (1988).
- [30] T. Tybell, P. Paruch, T. Giamarchi, and J.-M. Triscone, *Phys. Rev. Lett.* **89**, 097601 (2002).
- [31] J. Y. Jo, H. S. Han, J. G. Yoon, T. K. Song, S. H. Kim, and T. W. Noh, *Phys. Rev. Lett.* **99**, 267602 (2007).
- [32] J. Y. Jo, S. M. Yang, T. H. Kim, H. N. Lee, J. G. Yoon, S. Park, Y. Jo, M. H. Jung, and T. W. Noh, *Phys. Rev. Lett.* **102**, 045701 (2009).
- [33] M. Pešić, F. P. G. Fengler, L. Larcher, A. Padovani, T. Schenk, E. D. Grimley, X. Sang, J. M. LeBeau, S. Slesazeck, U. Schroeder *et al.*, *Adv. Funct. Mater.* **26**, 4601 (2016).
- [34] P. Erhart, P. Träskelin, and K. Albe, *Phys. Rev. B* **88**, 024107 (2013).
- [35] Y. Li, J. Li, R. Liang, R. Zhao, B. Xiong, H. Liu, H. Tian, Y. Yang, and T.-L. Ren, *Appl. Phys. Lett.* **114**, 142902 (2019).
- [36] S.-N. Choi, S.-E. Moon, and S.-M. Yoon, *Ceram. Int.* **45**, 22642 (2019).